Research Report

In situ imaging of mitochondrial outer-membrane pores using atomic force microscopy

Bradley E. Layton, Ann Marie Sastry, Christian M. Lastoskie, Martin A. Philbert, Terry J. Miller, Kelli A. Sullivan, Eva L. Feldman, and Chia-Wei Wang

BioTechniques 37:564-573 (October 2004)

Here we describe a technique for imaging of the outer contours of the mitochondrial membrane using atomic force microscopy, subsequent to or during a toxic or metabolic challenge. Pore formation in both glucose-challenged and 1,3-dinitrobenzene (DNB)-challenged mitochondria was observed using this technique. Our approach enables quantification of individual mitochondrial membrane pore formations. With this work, we have produced some of the highest resolution images of the outer contours of the in situ mitochondrial membrane published to date. These are potentially the first images of the component protein clusters at the time of formation of the mitochondrial membrane transition pore in situ. With the current work, we have extended the application of atomic force microscopy of mitochondrial membranes to fluid imaging. We have also begun to correlate 3-D surface features of mitochondria dotted with open membrane pores with features previously viewed with electron microscopy (EM) of fixed sections.

INTRODUCTION

Selective passage of solute molecules into and out of the cell is accomplished by several classes of pore-forming proteins that are integral to the cell membrane. An important subset of these channel-forming proteins are the porins (1), proteins that adopt a characteristic barrel-shaped configuration and form channels spanning the extracellular and intracellular environments (2,3) as shown in Figure 1. Porins are found in the outer membranes of Gram-negative bacteria and in the membranes of mitochondria and chloroplast organelles in eukaryotic cells (1); typical interior diameters at the constriction regions within porin channels are about 2 nm, which are sufficiently large to allow the passage of a number of low molecular weight solutes via diffusive transport (4). Nonetheless, a large number of membrane porins are required to accomplish significant transport. A typical bacterium, for example, is estimated to have 10^5 porins in its outer membrane (5).

Porins play a critical role in cellular and organellar transport processes. For example, in mitochondria, the formation of a large, multiprotein porin complex mediates either energy production capability (closed probability state) or cell death (open probability state) by preventing or permitting the exchange of matrix components with matrix and/or intermembrane components. Such exchange is critical to secondary cellular processes (6–8) and thus largely determines cell fate (9–13). Dozens of membrane channels have been identified to date, as summarized in Table 1 (Reference 1; a database of these channel-forming proteins may be found at http://saier-144-164.ucsd.edu/tcdb/). Selected α-helix and β-barrel pore-forming proteins, with occurrence, channel size, and permeable substrates for each membrane protein are shown in Table 2 (14–22). It should be noted that while certain transport proteins such as gramicidin form cylindrical channels that are well described by a single measure of internal pore width, many channel-forming proteins have internal pore cross sections that vary along the channel axis, with one or more internal cavities separated from extracellular and intracelluar vestibules by pore constrictions or gating regions. In such instances, effective pore radii for the "cavity" and "gate" regions have been reported (Table 2) as obtained via crystallography (20) or from estimates obtained from permeation measurements (21) or homology studies (22).

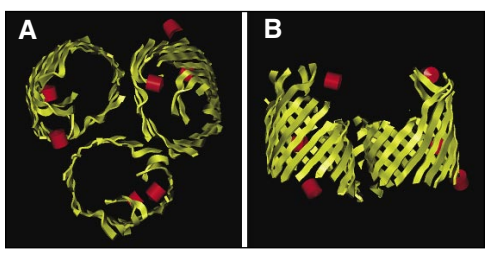

Figure 1. OmpF, a trimeric β-barrel porin. (A) Top view, and (B) side view. In panel B, the top of the protein opens to the extracellular domain, and the bottom of the protein opens to the intracellular domain. β strands are shown as ribbons and α-helices as red cylinders.

One much studied porin is the voltage-dependent, anion-selective channel porin (VDAC). This porin is found in the mitochondrial outer membranes of animal cells (23,24). It is selectively permeable to anions and can also undergo a transition to be selective to cation transport (9). The VDAC is also thought to play a key role in the regulation of mitochondrial-

University of Michigan, Ann Arbor, MI, USA

Table 1. Classifications of Channel-Forming Membrane Proteins with Their Occurrence, Function, and a Representative Protein from Each Class

Channel Type	Cell/Organelle Type	Function	Example Protein
α-helix bundle	bacteria, animal, and plant tissue cells, mitochondria	communication, homeostasis	K^+ channel
β-barrel porin	gram-negative bacteria, mitochondria, chloroplasts	general or specific transport across membrane	OmpF porin
holin	bacteria, viral pathogens	induce apoptosis	autolysin
protein toxin	bacteria, yeast, protozoa	nutrient leakage	colicin
peptide toxin	bacteria, animal cells	disrupt membrane	bee venom

mediated apoptosis. Specifically, it has been hypothesized to either coalesce into a megapore, the permeability transition pore (PTP), or alternatively, to close entirely, presumably resulting in heightened internal mitochondrial pressure. Either hypothesis would be consistent with mitochondrial rupture preceding the known release of cytochrome *c* and the resulting activation of irreversible cascades of apoptotic, intracellular "killer proteases" (e.g., Reference 25). Thus, both the opening and closure of the pore and the dimensions associated with each have been the subject of intense study.

The three-dimensional (3-D) shape of the VDAC pore has been determined to approximately 0.1 nm resolution (26), using sequence analysis and circular dichroism to find that the protein forms a structure similar to a bacterial porin-like β-barrel. Measured conductance of a membrane consisting of VDAC pores in a bilayer in the presence of molecules with diameters on the order of the pore inner diameter (27) was used to determine an inner diameter of 1.2–1.5 nm for the *Neurospora crassa* mitochondrial VDAC pore. An overall molecular weight of 34 kDa has also been obtained via Western blot analysis (28,29). The membrane has an approximate density of several thousand pores per square micrometer, as measured in bovine heart with enzyme-linked immunosorbent assay (ELISA) (30), and in the neurospora fungus using conductance measurements across membranes and using single-channel recordings (31). One of the

Table 2. Selected α-Helix and β-Barrel Pore-Forming Proteins, with Occurrence, Channel Size, and Permeable Substrates for Each Membrane Protein

Channel	Organism	Permeates	Radius (nm)	Reference
gramicidin	bacteria	H^+, Li^+, Na^+, K^+	0.2	Smart et al. (14)
KcsA	bacteria	K^+, Rb^+, Cs^+	0.1 (gate) 0.6 (cavity)	Doyle et al. (15) Allen et al. (16)
acetylcholine receptor	eukaryotes	glycine, serotonin	0.3 (gate) 2.0 (cavity)	Stein (17) Miyazawa et al. (18)
OmpF	bacterial outer membrane	nonselective for cations, anions, sugars, others	0.5 (gate) 1.8 (cavity)	Jap et al. (19) Schirmer (20)
VDAC	eukaryotic mitochondrial	similar to OmpF, but voltage-dependent anion selectivity	0.8 (gate) 1.3 (cavity)	Benz (21) Casadio et al. (22)

VDAC, voltage-dependent, anion-selective channel outer membrane porin.

functional implications of its inherent pore geometry is that VDAC is readily permeable to glucose, the latter of which has a diameter of <1 nm (32).

Atomic force microscopy (AFM) has been successfully applied to the imaging of biological surfaces, as demonstrated in the characterization of the general surface morphology of mitochondria (33–35), spermatozoa (36), and neurons (37). With its sub-nanometer resolution and its capability to image features in aqueous environments, AFM is also well suited to imaging organelle membrane proteins in situ (38) or in monolayers (39,40). Examples of previous imaging experiments on the mitochondrial outer-membrane structure with AFM include the use of immunologically labeled 8 nm gold particles conjugated to anti-rabbit immunoglobulin G (IgG) anti-PBR (peripheral-type benzodiazepine receptor) (29,38) and direct verification of the presence of mitochondria through the cell membrane of rat mammary carcinoma cells (34). Two other groups (41,42) have imaged mitochondrial-associated proteins directly, but did so in reconstituted lipid films, rather than in situ. The inner mitochondrial structure has been viewed via electron microscope (EM) tomography (43–45). One group (29) found that the hCG hormone caused rapid reorganization of the peripheral-type benzodiazepine receptor of unfixed mitochondria of Leydig tumor cells with AFM in air-contact mode using gold particles as labels. Another group (34) imaged fixed mitochondria in air-contact mode in partially fractured rat mammary carcinoma cells. Several reports (43–45) have described 5 nm resolution images, obtained by imaging a relatively thick (approximately 1 μm) section with a transmission electron microscope (TEM) at a series of angles and reconstructing the 3-D shape from the 2-D projections.

In the present study, we use a refined AFM approach to investigate mitochondrial pore formation subsequent to two specific types of challenge: excess glucose and 1,3-dinitrobenzene (DNB) exposure. Under both conditions, mitochondria swell as a result of water flux into the hypertonic matrix. Specific rationales follow for each case. This work combines a refined mitochondrial isolation protocol, followed immediately by either a metabolic or toxic challenge, while being tracked by AFM to determine structural changes in mitochondrial outer-membrane topology as evidenced by porin proliferation or reorganization. Two protocols are described: one in which mitochondria were isolated from embryonic rat primary dorsal root ganglion cells and subjected to a glucose challenge, and one in which adult rat liver mitochondria were isolated and subjected to a DNB challenge. These two preparations were imaged directly with AFM to a resolution sufficient to image mitochondrial membrane proteins in situ. To our knowledge, ours is the first work to image unlabeled mitochondrial membrane pores in situ with AFM subsequent to isolation from the cell and in conjunction with a toxic or metabolic challenge.

Glucose Challenge

Russell et al. (8) found that mitochondria from rat primary dorsal root ganglia (DRG) neurons challenged with 45 mM glucose for 6 h showed an increase in cross-sectional area of approximately 50% (0.43 ± 0.03 μm^2 vs. 0.66 ± 0.08 μm^2) by measuring maximal cross-sectional area through a z-series of a fluorescent signals under confocal microscopy. We can estimate that this comprises an 80% increase in volume, assuming an ellipsoidal shape for mitochondria ($V \propto A^{3/2}$). Mitochondrial swelling was found to be dose- and time-dependent, with increased glucose molarities resulting in greater swelling rates, and longer exposure resulting in greater volumetric increases (at 150 mM, 130% $\Delta A \rightarrow$ 350% ΔV; at 300 mM, 166% $\Delta A \rightarrow$ 440% ΔV) after 6 h. A plateau in cross-sectional area ($\Delta A \sim 120\% = \Delta V \sim 225\%$) as measured by confocal microcopy was apparently reached after 24 and 48 h of excessive (45 mM) glucose exposure. Swelling appeared to be coupled with the complete membrane depolarization (loss of $\Delta\Psi_{mt}$) at 24 h, as measured by a change in wavelength of a voltage-dependent fluorophore (8).

The precise mechanism for the disruption of excess glucose on the viability of mitochondria is not yet known, but likely involves disruption of the normal cycle of several proton-pumping inner-membrane proteins responsible for maintaining a negative voltage gradient between the intermembrane space and the matrix (46). Thus, it is likely that a change in the metabolic cycle results in a change in the electronegativity of the matrix, thus causing a change in osmotic pressure and producing swelling (47).

1,3-Dinitrobenzine/Cyclosporin-A

It has been observed by several separate groups that toxic challenge to mitochondria (e.g., exposure to DNB) triggers mitochondrial permeability transition (MPT), as marked by formation of a megapore, the mitochondrial permeability transition pore (mtPTP) at the inner membrane (48–50). This pore has not been directly imaged, although its presence has been verified using spatial distribution of fluorescent dyes, calcein and tetramethylrhodamine methy-

lester (TMRM) (51). Inner-membrane proteins such as adenine nucleotide translocase (ANT) and outer-membrane proteins such as VDAC are putative core components. Cyclosporin-A (CsA) is a well-known inhibitor of MPT pore formation (52) The mtPTP has been partially reconstituted in solution to test the hypothesis that the permeability transition pore may be formed from hexokinase, the enzyme responsible for catalyzing the transfer of phosphate to glucose, an outer-membrane porin, and the adenylate nucleotide translocator, an inner-membrane integral protein (53).

Novelty of Technique

Previously published AFM images of mitochondria used indirect methods (29,34,38), such as artificial membranes (41,42) or proteins outside of a membrane (33,37,54). Furthermore, the specific combination of our refinement of (55) technique for two separate tissue types combined with AFM is the first such application to the knowledge of the investigators.

MATERIALS AND METHODS

In both studies, mitochondria were isolated based on the mitochondrial isolation protocol of Verweij et al. (55). All procedures were executed in accordance with university, state, and federal standards in accord with the National Research Council's "Guide for the Care and Use of Laboratory Animals." These two isolation procedures are tissue-specific due to the relatively mitochondria high density and volume of tissue available in liver used in the DNB study compared to that of embryonic DRG cells used in the glucose-challenge study.

All imaging of preparations of mitochondria was performed using a NanoScope® III Dimension 3000 series BioScope® (Veeco Instruments, Woodbury, NY, USA) in air-contact, air-tapping, or fluid-tapping modes. For air-contact mode, Nanoprobe™ DNPS tips were used (Veeco Instruments). For air tapping mode, Metrology Probes™ (NanoDevices, Santa Barbara, CA, USA) were used at a frequency of approximately 290 kHz. For fluid-tapping mode, we used DNPS tips, employing the shortest cantilever of the four on the chip (approximately 100 μm) with the narrowest legs (approximately 10 μm) of spring constant 0.32 N/m. This allowed for an imaging frequency of approximately 10 kHz. Scan rates of 1 Hz were typically used. Initially, proportional gain was set to 0.6 and the integral gain to 0.8. In tapping mode, to minimize contact forces once engagement occurred, set point amplitude was increased toward drive amplitude until disengagement occurred, and then decreased until the tip just regained contact. Typical error signals were on the order of 1 nm, once the tip force had been minimized. With this refinement of previous AFM imaging work (e.g., Reference 33), individual membrane features were resolvable.

Glucose Challenge

A timed pregnant Sprague-Dawley rat (E15) was euthanized via sodium pentobarbital (100 mg/kg) overdose. Approximately 30 DRG were harvested per embryo, yielding approximately 500 DRG. Mitochondria were isolated using a protocol based on Verweij et al. (55) and modified as described. DRG were placed for 10 min in 0.25 M trypsin and centrifuged for 5 min at 2200× *g*. The pellet was resuspended in a 1 mL ice-cold isotonic buffer (250 mM sucrose, 0.5 M EDTA, 20 mM HEPES, 500 μM Na_3VO_4, pH 7.4) with protease inhibitors (aprotinin and leupeptin and phenylmethanesulfonyl fluoride). The solution was homogenized with a glass Dounce homogenizer (Fisher Scientific, Pittsburgh, PA, USA) on ice for 20 strokes. One mL ice-cold isotonic buffer and protease inhibitor were added, and the resulting solution was centrifuged at 900× *g* for 5 min at -4°C. Supernatant containing mitochondria was carefully transferred into an ultracentrifuge tube. Care was taken to avoid any nonmitochondrial contaminants from the pellet to be pipetted. The supernatant containing mitochondria was then centrifuged at 12,000× *g* for 8 min. A small visible pellet was resolvable at this point. The supernatant was poured off and the pellet resuspended in 1 mL of ice-cold isotonic buffer (0.1 M sodium cacodylate in distilled water, of pH

7.4) without protease inhibitors. The solution was recentrifuged at 12,000× *g* for 8 min. A pellet was again visible. This final pellet was resuspended in 150 µL of ice-cold isotonic buffer (250 mM sucrose, 0.5 M EDTA, 20 mM HEPES, pH 7.4, 500 µM Na_3VO_4). Four 5 µL samples were pipetted into 1 mL tubes. The final yield was on the order of approximately 100 mitochondria per microliter. Two of these were glucose-challenged with 40 mM glucose for 6 h. At the end of 6 h, one of the glucose-challenged and one of the nonchallenged preparations were each fixed with 4% paraformadehyde in preparation for AFM.

1,3-Dinitrobenzine/Cyclosporin-A

Mitochondria from the liver of a male Fisher rat were prepared in a manner similar to that of Verweij et al. (55); the resulting mitochondrial pellet was resuspended in 1 mL of 250 mM sucrose solution. From this, 100 µL of mitochondria were withdrawn and distributed into several treatment tubes [DNB alone, DMSO (dimethyl sulfoxide; vehicle), and CsA pretreated/DNB]. The final concentration of DNB used was 100 µM (60 min treatment), and final concentration of CsA was 1 µM (30 min pretreatment). Mitochondria were resuspended in the high sucrose solution to ensure retention of viability. A portion was reserved and fixed with 4% paraformaldehyde in 0.1 M cacodylate buffer. The presence of mitochondria was verified by the addition of 100 nM MitoTracker® Green (Molecular Probes, Eugene, OR, USA) at 490 nm and detection at 516 nm on a Microphot microscope (Nikon, Melville, NY, USA) within 10 min of staining. Images were captured on a SPOT-RT digital camera (Diagnostic Instruments, Sterling Heights, MI, USA).

Three 1 mL samples were pipetted into 15 mL tubes. The final yield was greater than that of the glucose-challenged: approximately 1000 mitochondria per microliter were seen. One tube containing mitochondria was pretreated for 30 min with 1 µM CsA prior to treatment as previously described (48). After 1 h, each of the three preparations was fixed in 4% paraformaldehyde in cacoldylate buffer to ensure retention of organelle morphology prior to examination by AFM. Samples of 1 µL were deposited on mica (air) poly-L-lysine (fluid) Biocoat®-coated glass slides (Becton-Dickinson, Franklin Lakes, NJ, USA). Samples prepared for fluid tapping were immersed throughout preparation and imaging.

During imaging, regions containing features resembling mitochondria or mitochondrial clusters were selected and imaged at a resolution of 256 × 256 pixels over a region of approximately 40 × 40 µm at a scan rate of approximately 1 Hz. Within these regions, individual mitochondria were selected and imaged at a resolution of 512 × 512, also at a rate of approximately 1 Hz. This imaging speed was found to minimize thermal drift caused by expected pore mobility within the outer membrane, as well as deformation and displacement of the mitochondrion being imaged. This particular aspect of imaging membrane proteins in situ is critical for obtaining the best possible image because a series of images collected for offline autocorrelation is not possible due to the dynamic nature of the outer membrane. Specifically, with in situ imaging, when returning to the same coordinates or when rastering back-and-forth over the same region, subsequent images invariably differ from previous images.

RESULTS

The DNB/CsA liver preparation produced a greater number and more densely clustered mitochondria than that of the DRG preparation on both mica and poly-L-lysine surfaces (Figure 2).

Glucose-Challenged

Approximately 20 mitochondria were imaged from a total of 4 samples. In fluid-tapping mode, 10 mitochondria were imaged. Those which revealed the best-preserved overall morphology were the fixed; the unfixed, glucose-challenged mitochondria lost their morphology over the course of imaging.

At the whole-mitochondria scale, surface topology was visible (Figure 3A). The image shown is representative of those obtained; artificial lighting and coloring were used to enhance topological features. The exact shape of the interface between the mitochondria and the substrate is not known, so a deconvolution is not reliable in this case, but approximate mitochondria volume has been estimated to be on the order of 100 aL (1 aL = 100 nm^3).

On mitochondrial surfaces in control preparations, no finely structured features were evident (Figure 4A). Features of the same scale of VDAC were apparent, however, in the glucose-chal-

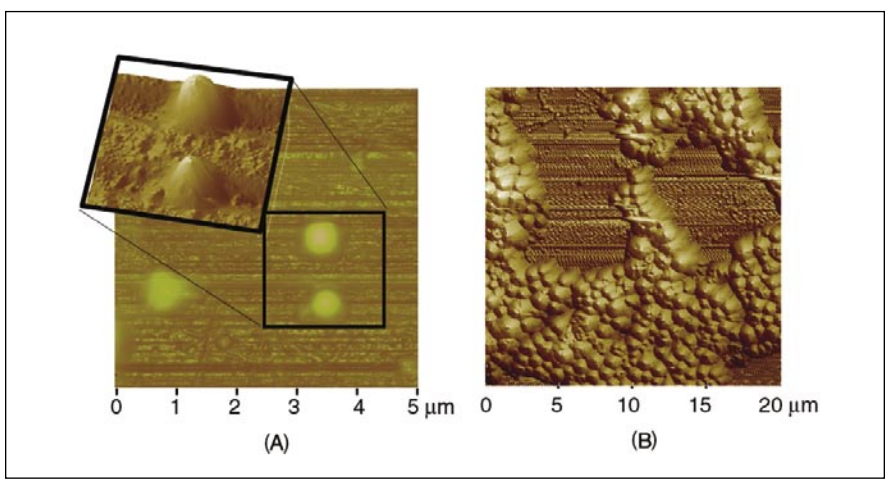

Figure 2. Clustering of fixed mitochondria on mica resulting from two preparation techniques. (A) A 5-µm air-contact atomic force microscopy (AFM) image of glucose-challenged mitochondria from embryonic Sprague-Dawley rat dorsal-root ganglion neurons, showing a relatively sparse concentration of mitochondria. (B) A 20-µm air-tapping AFM image of 1,3-dinitrobenzene (DNB)-challenged mitochondria from Fisher rat liver, showing significant clustering of mitochondria. The pyramidal shape of the mitochondria in both panels is a result of the interaction with the pyramidal tip with four 35˚ sides, a nominal height of 10 µm, and a tilt of 10˚ from horizontal.

lenged mitochondria. Some imaging artifacts arose (e.g., horizontal streaking within scan lines), but the organization of membrane proteins appeared visible. Periodic invaginations of approximately 5 nm were present (typical image shown in Figure 4B). To the authors' knowledge, this is the first such imaging of a possible VDAC on a mitochondrial surface. Due to our limited sample sizes, however, full quantification of pore-like features has not yet been made.

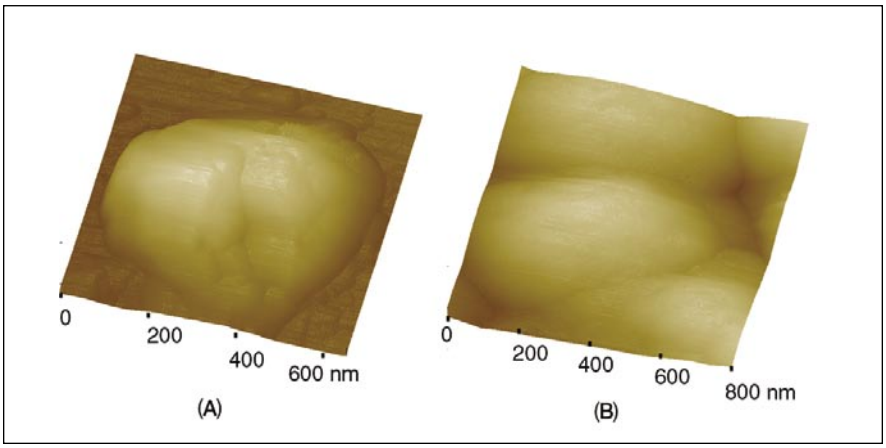

Figure 3. Air atomic force microscopy (AFM) images of fixed, glucose-, and 1,3-dinitrobenzene (DNB)-challenged mitochondrial surfaces. (A) Air-contact AFM image of glucose-challenged, Sprague-Dawley rat embryonic dorsal root ganglion neuronal mitochondrion. (B) Air-tapping AFM image of three adjacent, fixed, DNB-challenged, Fisher rat liver mitochondria. Surface features of approximately 10 nm are evident. The invaginations in the outer membrane may reveal the topography of the inner membrane.

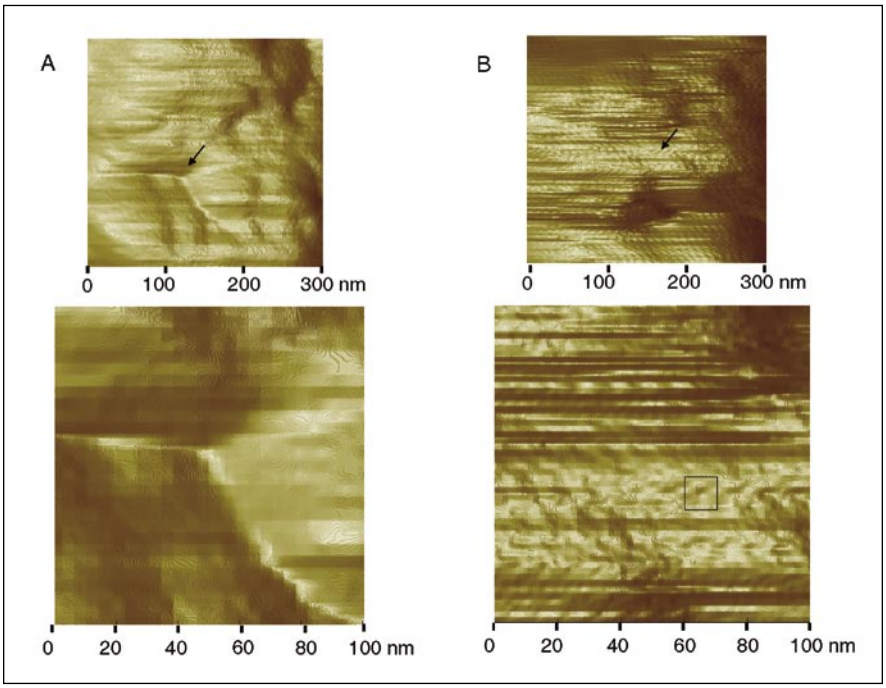

Figure 4. Fluid-tapping atomic force microscopy (AFM) images of fixed, control, and glucose-challenged Sprague-Dawley embryonic DRG mitochondria. (A) The 256×256 pixel (approximately 4 nm per pixel) image of an unchallenged outer membrane, revealing features of 10–100 nm. The indentation in the middle of the upper image may reveal topography of the inner membrane; a cropped portion of the upper image is shown in the lower image. (B) The 512×512 (approximately 2 nm per pixel) image of a glucose-challenged outer membrane, revealing invaginated features that may be VDAC pores; a cropped portion of the upper image is shown in the lower image. DNB, 1,3-dinitrobenzene; VDAC, voltage-dependent, anion-selective channel porin.

1,3-Dinitrobenzene-Challenged

In general, the surface roughness of DNB-challenged mitochondria was greater than that of either control or DNB-CsA treated mitochondria. The single DNB-challenged mitochondrion surface shown in Figure 3B represents a typical image. Clustering in the rat liver preparation was common, perhaps due to the higher yield relative to the DRG preparation.

In the unchallenged preparations, few features were resolvable on the mitochondrial surface; Figure 5A represents a typical image. The single bulge evident in this image was typical and may have resulted from the protrusion of the inner membrane through the outer membrane. It seems likely that if the tip had traversed a pore during imaging, that a 2–3 nm inner pore diameter would be evident due to the interaction. Challenged preparations revealed altered mitochondrial surfaces; a typical image is shown as Figure 5B. This surface appears to contain a pore-like structure of dimensions consistent with a mitochondrial permeability transition pore. When contrasted to the control image (Figure 5A), similar features are found but are not as pronounced. A complete statistical analysis of data was not performed due to small sample sizes, but typical images are shown.

DISCUSSION

With this work, we have presented some of the highest resolution images of the outer contours of the mitochondrial membrane published to date. These are potentially the first images of the component protein clusters at the time of formation of the mitochondrial membrane transition pore (Figure 5B). This structure could form via radial expansion, wherein concentric rings form and successively collapse, until a "megapore" of approximately 30 nm results. This may involve N terminus to C terminus bindings between adjacent porins, as illustrated in Figure 1. An alternative hypothesis is that the structures seen in Figure 5B are those similar to those seen by Kiselyova et al. (56).

One particular challenge for obtaining optimally resolved AFM images is to balance the competing effects of the amount of time spent collecting data from a given location (slow scanning) and the amount of thermal drift that can occur over the course of a single scan or even between sequential fast-raster movements. The challenge becomes greater when imaging on the top of deformable adsorbed organelles. The challenge may be likened to trying to resolve the individual nubs on a partially flattened basketball without moving the ball itself. Though individual biomolecules have been successfully imaged in membranes or other substrates (57–59), imaging of membrane proteins directly on cells presents an additional challenge.

Convolution artifact plays a role in AFM by distorting the image of the structures one views. In the present study, this effect can be seen in the large scan as evidenced by the pyramidal appearance of the mitochondria. There is also some artifact due to the finite radius of the tip; however, accurate horizontal information is obtainable if one is measuring the distance between two peaks because the lowest point of the tip must touch the highest point(s) of the sample.

From this work, we may begin to approximate transport rates that must be present during a pore opening, given variables such as pore diameter and molecular species of transport. Potentially, the rate at which mitochondrial swelling occurs as a precursor to apoptosis and correlates with loss of outer-membrane potential can be measured with this method. While this method is somewhat artificial in that it does not allow observation of mitochondrial behavior as it might occur within a living cell (60), it has the advantage of viewing the membrane directly during a toxic challenge and the potential for the identification of specific proteins involved in the stabilization/destabilization of the pore complex.

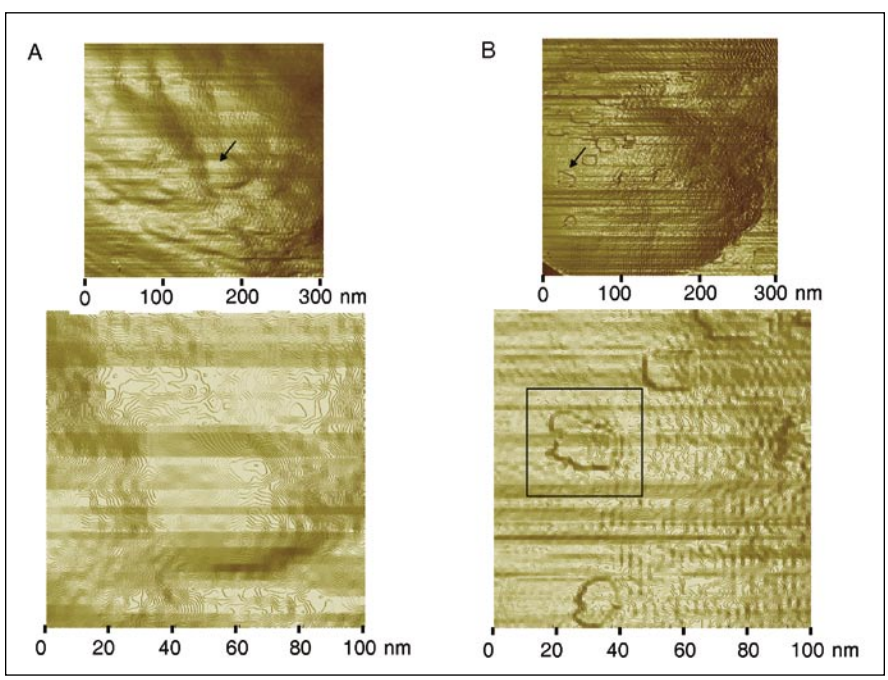

Figure 5. Fluid-tapping atomic force microscopy (AFM) images of fixed, control, and DNB-challenged Fisher rat liver mitochondria. (A) The 512 × 512 pixel (approximately 2 nm per pixel) image of a control Fisher rat liver mitochondrial outer membrane, revealing surface features 10–20 nm. (B) The 512 × 512 pixel (approximately 2 nm per pixel) image of a DNB-challenged mitochondrial outer membrane, showing large openings with diameters of approximately 10–20 nm, suggesting presence of permeability transition pores; an enlargement is shown in the lower image. These larger features are absent in panel A. DNB, 1,3-dinitrobenzene.

Clustering on Preparations

This clustering behavior could be related to that seen by Yaffe (61), whose work describes the many specialized and reticulated shapes that mitochondria or groups of mitochondria may

form in various cells, such as sperm cells and muscle cells, as apparently dictated by the dynamin protein Dnm1 and the fuzzy onion protein Fzo1, both outer-membrane associated proteins with still unknown control mechanisms. At this large scale, taken at a resolution of 512 × 512 nm, no surface features can be seen, and tip artifact consisting of a pyramidal appearance is present.

With the current work, we have extended the work of atomic force microscopists by imaging in fluid as well as in air and have begun to interpret the physical landscape of mitochondria dotted with open membrane pores, in relation to those imaged using EM tomography of fixed sections.

FUTURE WORK

The qualification of the pore type will hopefully give a snapshot of the condition of the pore upon fixation and support one of three different possible pore-formation mechanisms. These include: first, a more or less random "pore flicker" event during which the inner and outer pore components are briefly aligned, implying a completely entropy-driven process; second, a semi-random, or partially controlled formation, implying transitory conformational changes driven by either abrupt changes in electrochemical gradients or changes in mechanical states such as intermembrane pressure or relative strains between membranes; or third, a more permanent pore with perhaps a spoke-and-hook structure.

In general, membrane pore geometry is critical to understanding both the types of molecules that may pass through the outer membrane as well as the evolutionary origins of porins (1). The putative symbiotic evolution of bacterial cells as mitochondrial organelles within eukaryotic cells provides an explanation for the structural homology between bacterial and mitochondrial porin channels (21). This similarity can be exploited to infer mitochondrial membrane transport characteristics from computational and experimental investigations of diffusive transport in bacterial outer-membrane porins, which will also be part of future work.

ACKNOWLEDGMENTS

We are grateful for the assistance in mitochondrial preparations performed by Hui Wang, Carey Backus, and John Hayes. Major funding for this work was provided by the W.M. Keck Foundation. Additional funding from NSF PECASE (A.M.S.) and NSF CAREER (C.M.L.) grants, along with the National Institutes of Health grant no. NIH-R01 ES08846 (M.A.P.) and the Juvenile Diabetes Research Foundation Center for the Study of Complications in Diabetes (E.F. and K.A.S.) also supported this work.

COMPETING INTERESTS STATEMENT

The authors declare no competing interests.

REFERENCES

1. **Saier, M.H., Jr.** 2000. Families of proteins forming transmembrane channels. J. Membr. Biol. *175*:165-180.
2. **Brdiczka, D., G. Beutner, A. Ruck, M. Dolder, and T. Wallimann.** 1998. The molecular structure of mitochondrial contact sites. Their role in regulation of energy metabolism and permeability transition. Biofactors *8*:235-242.
3. **Schatz, G. and B. Dobberstein.** 1996. Common principles of protein translocation across membranes. Science *271*:1519-1526.
4. **Schulz, G.E.** 1996. Porins: general to specific, native to engineered passive pores. Curr. Opin. Struct. Biol. *6*:485-490.
5. **Buechner, M., A.H. Delcour, B. Martinac, J. Adler, and C. Kung.** 1990. Ion channel activities in the Escherichia coli outer membrane. Biochim. Biophys. Acta *1024*:111-121.
6. **Kroemer, G. and J.C. Reed.** 2000. Mitochondrial control of cell death. Nat. Med. *6*:513-519.
7. **Petersen, K.F., D. Befroy, S. Dufour, J. Dziura, C. Ariyan, D.L. Rothman, L. DiPietro, G.W. Cline, et al.** 2003. Mitochondrial dysfunction in the elderly: possible role in insulin resistance. Science *300*:1140-1142.
8. **Russell, J.W., D. Golovoy, A.M. Vincent, P. Mahendru, J.A. Olzmann, A. Mentzer, and E.L. Feldman.** 2002. High glucose-induced oxidative stress and mitochondrial dysfunction in neurons. FASEB J. *16*:1738-1748.
9. **Vander Heiden, M.G., N.S. Chandel, X.X. Li, P.T. Schumacker, M. Colombini, and C.B. Thompson.** 2000. Outer mitochondrial membrane permeability can regulate coupled respiration and cell survival. Proc. Natl. Acad. Sci. USA *97*:4666-4671.
10. **Robertson, J.D., B. Zhivotovsky, V. Gogvadze, and S. Orrenius.** 2003. Outer mitochondrial membrane permeabilization: an open-and-shut case? Cell Death Differ. *10*:485-487.
11. **Bernardi, P., R. Colonna, P. Costantini, O. Eriksson, E. Fontaine, F. Ichas, S. Massari, A. Nicolli, et al.** 1998. The mitochondrial permeability transition. Biofactors *8*:273-281.
12. **Halestrap, A.P., P.M. Kerr, S. Javadov, and K.Y. Woodfield.** 1998. Elucidating the molecular mechanism of the permeability transition pore and its role in reperfusion injury of the heart. Biochim. Biophys. Acta *1366*:79-94.
13. **He, L. and J.J. Lemasters.** 2002. Regulated and unregulated mitochondrial permeability transition pores: a new paradigm of pore structure and function? FEBS Lett. *512*:1-7.
14. **Smart, O.S., J.M. Goodfellow, and B.A. Wallace.** 1993. The pore dimensions of gramicidin A. Biophys. J. *65*:2455-2460.
15. **Doyle, D.A., J. Morais Cabral, R.A. Pfuetzner, A. Kuo, J.M. Gulbis, S.L. Cohen, B.T. Chait, and R. MacKinnon.** 1998. The structure of the potassium channel: molecular basis of K+ conduction and selectivity. Science *280*:69-77.
16. **Allen, T.W., A. Bliznyuk, A.P. Rendell, S. Kuyucak, and S.H. Chung.** 2000. The potassium channel: structure, selectivity and diffusion. J. Chem. Phys. *112*:8191-8204.
17. **Stein, W.D.** 1990. Channels, Carriers, and Pumps: an Introduction to Membrane Transport, p. 80,94. Academic Press, San Diego.
18. **Miyazawa, A., Y. Fujiyoshi, M. Stowell, and N. Unwin.** 1999. Nicotinic acetylcholine receptor at 4.6 A resolution: transverse tunnels in the channel wall. J. Mol. Biol. *288*:765-786.
19. **Jap, B.K. and P.J. Walian.** 1996. Structure and functional mechanism of porins. Physiol. Rev. *76*:1073-1088.
20. **Schirmer, T.** 1998. General and specific porins from bacterial outer membranes. J. Struct. Biol. *121*:101-109.
21. **Benz, R.** 1994. Permeation of hydrophilic solutes through mitochondrial outer membranes: review on mitochondrial porins. Biochim. Biophys. Acta *1197*:167-196.
22. **Casadio, R., I. Jacoboni, A. Messina, and V. De Pinto.** 2002. A 3D model of the voltage-dependent anion channel (VDAC). FEBS Lett. *520*:1-7.
23. **Dihanich, M.** 1990. The biogenesis and function of eukaryotic porins. Experientia *46*:146-153.
24. **Muller, D.J., H. Janovjak, T. Lehto, L. Kuerschner, and K. Anderson.** 2002. Observing structure, function and assembly of single proteins by AFM. Prog. Biophys. Mol. Biol. *79*:1-43.
25. **Martinou, J.C., S. Desagher, and B. Antonsson.** 2000. Cytochrome c release from mitochondria: all or nothing. Nat. Cell Biol. *2*:E41-E43.
26. **Mannella, C.A.** 1998. Conformational changes in the mitochondrial channel protein, VDAC, and their functional implications. J. Struct. Biol. *121*:207-218.
27. **Rostovtseva, T.K., A. Komarov, S.M. Bezrukov, and M. Colombini.** 2002. VDAC channels differentiate between natural metabolites and synthetic molecules. J. Membr. Biol. *187*:147-156.

28. **Garnier, M., A. Dimchev, N. Boujrad, M.J. Price, N.A. Musto, and V. Papadopoulos.** 1994. In vitro reconstitution of a functional peripheral-type benzodiazepine receptor. Mol. Pharmacol. *45*:201-211.
29. **Boujrad, N., B. Vidic, and V. Papadopoulos.** 1996. Acute action of choriogonadotropin on Leydig tumor cells: changes in the topography of the mitochondrial peripheral-type benzodiazepine receptor. Endocrinology *137*:5727-5730.
30. **De Pinto, V., G. Prezioso, F. Thinnes, T.A. Link, and F. Palmieri.** 1991. Peptide-specific antibodies and proteases as probes of the transmembrane topology of the bovine heart mitochondrial porin. Biochemistry *30*:10191-10200.
31. **Freitag, H., W. Neupert, and R. Benz.** 1982. Purification and characterisation of a pore protein of the outer mitochondrial membrane from Neurospora crassa. Eur. J. Biochem. *123*:629-636.
32. **Nitzan, Y., K. Orlovsky, and I. Pechatnikov.** 1999. Characterization of porins isolated from the outer membrane of Serratia liquefaciens. Curr. Microbiol. *38*:71-79.
33. **Wagner, O.I., J. Lifshitz, P.A. Janmey, M. Linden, T.K. McIntosh, and J.F. Leterrier.** 2003. Mechanisms of mitochondria-neurofilament interactions. J. Neurosci. *23*:9046-9058.
34. **Pietrasanta, L.I., A. Schaper, and T.M. Jovin.** 1994. Imaging subcellular structures of rat mammary carcinoma cells by scanning force microscopy. J. Cell Sci. *107(Pt 9)*:2427-2437.
35. **Kordylewski, L., D. Saner, and R. Lal.** 1994. Atomic force microscopy of freeze-fracture replicas of rat atrial tissue. J. Microsc. *173(Pt 3)*:173-181.
36. **Joshi, N.V., H. Medina, C. Colasante, and A. Osuna.** 2000. Ultrastructural investigation of human sperm using atomic force microscopy. Arch. Androl. *44*:51-57.
37. **Parpura, V., P.G. Haydon, and E. Henderson.** 1993. Three-dimensional imaging of living neurons and glia with the atomic force microscope. J. Cell Sci. *104(Pt 2)*:427-432.
38. **Papadopoulos, V., N. Boujrad, M.D. Ikonomovic, P. Ferrara, and B. Vidic.** 1994. Topography of the Leydig cell mitochondrial peripheral-type benzodiazepine receptor. Mol. Cell Endocrinol. *104*:R5-R9.
39. **Neff, D., S. Tripathi, K. Middendorf, H. Stahlberg, H.J. Butt, E. Bamberg, and N.A. Dencher.** 1997. Chloroplast F0F1 ATP synthase imaged by atomic force microscopy. J. Struct. Biol. *119*:139-148.
40. **Schillers, H., T. Danker, H.J. Schnittler, F. Lang, and H. Oberleithner.** 2000. Plasma membrane plasticity of Xenopus laevis oocyte imaged with atomic force microscopy. Cell Physiol. Biochem. *10*:99-107.
41. **Ding, T.T., S.J. Lee, J.C. Rochet, and P.T. Lansbury, Jr.** 2002. Annular alpha-synuclein protofibrils are produced when spherical protofibrils are incubated in solution or bound to brain-derived membranes. Biochemistry *41*:10209-10217.
42. **Epand, R.F., J.C. Martinou, S. Montessuit, R.M. Epand, and C.M. Yip.** 2002. Direct evidence for membrane pore formation by the apoptotic protein Bax. Biochem. Biophys. Res. Commun. *298*:744-749.
43. **Frey, T.G. and C.A. Mannella.** 2000. The internal structure of mitochondria. Trends Biochem. Sci. *25*:319-324.
44. **Mannella, C.A., K. Buttle, B.K. Rath, and M. Marko.** 1998. Electron microscopic tomography of rat-liver mitochondria and their interaction with the endoplasmic reticulum. Biofactors *8*:225-228.
45. **Perkins, G., C. Renken, M.E. Martone, S.J. Young, M. Ellisman, and T. Frey.** 1997. Electron tomography of neuronal mitochondria: three-dimensional structure and organization of cristae and membrane contacts. J. Struct. Biol. *119*:260-272.
46. **Lamson, D.W. and S.M. Plaza.** 2002. Mitochondrial factors in the pathogenesis of diabetes: a hypothesis for treatment. Altern. Med. Rev. *7*:94-111.
47. **Vander Heiden, M.G., N.S. Chandel, E.K. Williamson, P.T. Schumacker, and C.B. Thompson.** 1997. Bcl-xL regulates the membrane potential and volume homeostasis of mitochondria. Cell *91*:627-637.
48. **Phelka, A.D., M.J. Beck, and M.A. Philbert.** 2003. 1,3-Dinitrobenzene inhibits mitochondrial complex II in rat and mouse brainstem and cortical astrocytes. Neurotoxicology *24*:403-415.
49. **Haworth, R.A. and D.R. Hunter.** 1979. The Ca2+-induced membrane transition in mitochondria. II. Nature of the Ca2+ trigger site. Arch. Biochem. Biophys. *195*:460-467.
50. **Hunter, D.R. and R.A. Haworth.** 1979. The Ca2+-induced membrane transition in mitochondria. I. The protective mechanisms. Arch. Biochem. Biophys. *195*:453-459.
51. **Lemasters, J.J., A.L. Nieminen, T. Qian, L.C. Trost, and B. Herman.** 1997. The mitochondrial permeability transition in toxic, hypoxic and reperfusion injury. Mol. Cell. Biochem. *174*:159-165.
52. **Friberg, H. and T. Wieloch.** 2002. Mitochondrial permeability transition in acute neurodegeneration. Biochimie *84*:241-250.
53. **Beutner, G., A. Ruck, B. Riede, and D. Brdiczka.** 1998. Complexes between porin, hexokinase, mitochondrial creatine kinase and adenylate translocator display properties of the permeability transition pore. Implication for regulation of permeability transition by the kinases. Biochim. Biophys. Acta *1368*:7-18.
54. **Davis, J.J., H.A. Hill, and T. Powell.** 2001. High resolution scanning force microscopy of cardiac myocytes. Cell. Biol. Int. *25*:1271-1277.
55. **Verweij, B.H., J.P. Muizelaar, F.C. Vinas, P.L. Peterson, Y. Xiong, and C.P. Lee.** 1997. Mitochondrial dysfunction after experimental and human brain injury and its possible reversal with a selective N-type calcium channel antagonist (SNX-111). Neurol. Res. *19*:334-339.
56. **Kiselyova, O.I., I.V. Yaminsky, Y.D. Ivanov, I.P. Kanaeva, V.Y. Kuznetsov, and A.I. Archakov.** 1999. AFM study of membrane proteins, cytochrome P450 2B4, and NADPH-cytochrome P450 reductase and their complex formation. Arch. Biochem. Biophys. *371*:1-7.
57. **Moller, C., M. Allen, V. Elings, A. Engel, and D.J. Muller.** 1999. Tapping-mode atomic force microscopy produces faithful high-resolution images of protein surfaces. Biophys. J. *77*:1150-1158.
58. **Muller, D.J., M. Amrein, and A. Engel.** 1997. Adsorption of biological molecules to a solid support for scanning probe microscopy. J. Struct. Biol. *119*:172-188.
59. **Muller, D.J., C.A. Schoenenberger, F. Schabert, and A. Engel.** 1997. Structural changes in native membrane proteins monitored at subnanometer resolution with the atomic force microscope: a review. J. Struct. Biol. *119*:149-157.
60. **Petronilli, V., G. Miotto, M. Canton, R. Colonna, P. Bernardi, and F. Di Lisa.** 1998. Imaging the mitochondrial permeability transition pore in intact cells. Biofactors *8*:263-272.
61. **Yaffe, M.P.** 1999. Dynamic mitochondria. Nat. Cell Biol. *1*:E149-E150.

Received 14 April 2004; accepted 7 July 2004.

Address correspondence to:

Professor Ann Marie Sastry
2250 G.G. Brown Building
2350 Hayward Street
Department of Mechanical Engineering/
Department of Biomedical Engineering
University of Michigan
Ann Arbor, MI 48109-2125
e-mail: amsastry@umich.edu